Available online at www.sciencedirect.com
SCIENCE DIRECT®
Nuclear Instruments and Methods in Physics Research A 556 (2006) 246–258
NUCLEAR INSTRUMENTS & METHODS IN PHYSICS RESEARCH Section A
www.elsevier.com/locate/nima

A new highly segmented start counter for the CLAS detector

Y.G. Sharabian[a], M. Battaglieri[c], V.D. Burkert[a], R. DeVita[c], L. Elouadrhiri[a], L. Guo[a], D. Kashy[a], V. Kubarovsky[b], G.S. Mutchler[e,*], M. Ostrick[f], M. Ripani[c], P. Rossi[d], A. Rottura[c], E. Pasyuk[g], D. Weygand[a]

[a]*Thomas Jefferson National Accelerator Facility, Newport News, VA 23606, USA*
[b]*Rensselaer Polytechnic Institute, Troy, NY 12180 and Thomas Jefferson National Accelerator Facility, Newport News, VA 23606, USA*
[c]*INFN Sezione di Genova, 16146 Genova, Italy*
[d]*INFN Laboratori Nazionali di Frascati, 00044 Frascati, Italy*
[e]*T.W. Bonner Nuclear Laboratory, Rice University, Houton, TX 77251-1892, USA*
[f]*Physikalisches Institut, Universität Bonn, Bonn, Germany*
[g]*Arizona State University, Tempe, AZ, 85287-1504, USA*

Received 26 July 2005; received in revised form 18 October 2005; accepted 19 October 2005
Available online 15 November 2005

Abstract

The design, construction and performance of a highly segmented Start Counter are described. The Start Counter is an integral part of the trigger used in photon beam running with CLAS in Hall B at the Thomas Jefferson National Accelerator Facility (TJNAF). The Start Counter is constructed of 24 2.2-mm-thick single-ended scintillation paddles, forming a hermetic hexagon around the target region. This device measures the interaction time of the incoming photon in the target by detecting the outgoing particles. The counter provides complex trigger topologies, shows good efficiency and achieved a time resolution of 350 ps.

PACS: 29.40.Mc

Keywords: CLAS; Plastic scintillator; Time-of-flight; Trigger

1. Introduction

The Continuous Electron Beam Accelerator at the Thomas Jefferson National Accelerator Facility currently delivers a continuous electron beam up to ~6 GeV in energy. The machine delivers beam to three experimental areas (Halls A, B, and C) at any multiple of $\frac{1}{5}$ of the endpoint energy. The beam has a 2.004 ns bunch structure with an energy spread of $\Delta E/E \leqslant 10^{-4}$. Hall B contains the CEBAF Large Acceptance Spectrometer (CLAS) [1]. CLAS is based on a multigap magnet with six superconducting coils, symmetrically arranged to generate an approximately toroidal field distribution. Each of the six sectors is instrumented with drift chambers [2] to determine charged particle trajectories, scintillation counters for the measurement of time-of-flight (TOF) [3], gas Cherenkov counters [4] for electron identification and an electromagnetic calorimeter [5] for electron, photon and neutron energy measurement and detection. A photon beam with energy resolution of $\Delta E_\gamma/E_\gamma = 10^{-3}$ is provided by the photon tagging system [6] upstream of the CLAS detector. The system tags photons with energies between 0.2 and 0.95 of the incident electron energy, E_0, using a scintillator hodoscope. The energy is measured using 384 plastic scintillators, E-counters, 20 cm long and 4 mm thick. Their widths range from 6 to 18 mm in order to subtend approximately constant momentum intervals of $0.003 \times E_0$. Each counter overlaps its adjacent neighbors by one-third of their respective widths, thus creating 767 energy bins that provide a resolution of $0.001 \times E_0$. The timing of the radiating electron is provided by a second plane of 61 T-counters 20 cm downstream of the E-counters, sized to give approximately equal counting rates over the range of

*Corresponding author. Tel.: +1 71 334 85315; fax: +1 71 334 85215.
E-mail address: mutchler@rice.edu (G.S. Mutchler).

0168-9002/$ - see front matter © 2005 Elsevier B.V. All rights reserved.
doi:10.1016/j.nima.2005.10.031

detected energy. These scintillators are 2 cm thick and read out using PMT's attached by solid light guides at both ends, giving a timing resolution of about 110 ps.

The main technique for particle identification in CLAS is through the measurement of the time-of-flight of the scattered particle from the interaction vertex to the outer detectors (TOF or EC). The time of interaction is obtained by determining the photon beam bucket that produced the event. For this purpose a sub-nanosecond coincidence of the tagging spectrometer with a counter (Start Counter) close to the target region is needed. The time of interaction at the target must be determined to ± 2 ns. The software-corrected time should result in a confidence interval between ± 1 ns for the interaction of greater than 99%, i.e. have tails outside of 1 ns for no more than 1% of the events. For a Gaussian time distribution, this translates into a standard deviation $\sigma = 388$ ps. Thus, the Start Counter signal in coincidence with the T-counter time allows good identification of the RF bucket that produced the hadronic interaction in the target. Comparison to the nearest RF time gives the start time of the particle trajectory to better than 25 ps.

Thin scintillators are required to minimize the effects of multiple scattering. In the old Start Counter design [7], there were two main contributions to the multiple scattering: The 2-mm-thick carbon fiber beam pipe surrounding the target, and the Start Counter scintillators. To keep the multiple scattering angle due to the Start Counter below that generated by the target and beam pipe ($\sim$1.5 mrad) the scintillators were 3 mm thick. A double-ended scintillator design was used to achieve the best timing. However, the PMTs could not be placed downstream of the Start Counter because they would interfere with the small angle acceptance of the CLAS or be subjected to an intense and potentially damaging photon flux. This led to a coupled paddle design [8]. In this design, adjacent paddles are mechanically joined at the downstream end to form three double-ended paddles covering all six sectors.

Although this design worked well for the initial low-intensity (<10 nA) running of the CLAS, it proved to be inadequate for the high-intensity running (e.g. >40 nA) that is needed for low cross-section experiments such as Pentaquark searches [9]. The scintillator signals began to "sag" under the increased count rate due to the current limitations of the PMT bases used, and the ability to form triggers with several particles in the final state was severely limited. In addition, the increasing multiple hits in the coupled paddles severely degraded the timing resolution. A new more highly segmented Start Counter was needed. With the increase in segmentation, the smaller width of the scintillators results in better light collection. This allows the use of thinner single-ended scintillators. With a new and improved support system the counter could be made more hermetic, provided the gap between the scintillators could be kept to a minimum. Finally, at these higher currents, the rate limits of the tagger were being reached so increasing the beam current was impractical. Thus, increasing the luminosity required a longer target, which necessitated a longer Start Counter to cover the desired acceptance.

2. New Start Counter

The new Start Counter was designed to provide full acceptance coverage defined by the CLAS detector with a 40 cm long liquid hydrogen target. Based on the estimated integrated rate load at the anticipated luminosity, the number of paddles has been chosen to be 24. According to Monte Carlo simulations [10], this segmentation is enough to keep the rate due to electromagnetic background within acceptable values by requiring the multiplicity of hit paddles to be equal or greater than two. The Start Counter, shown in Fig. 1, is built of six identical sectors surrounding the target cell mounted on a foam scattering chamber. Each sector consists of four EJ-200 scintillator paddles coupled to an acrylic light guide. A paddle is a continuous single piece of scintillator with a straight section 502 mm long, between two bends, and a tapered end, the "nose" (Fig. 2). The paddles were 29 mm wide and 2.15 mm thick, which along with the wrapping and the support material give a total thickness of about 0.26 g/cm^2. The two paddles in Fig. 2 along with their mirror images make up one sector. The first bend, which couples to the light guide, is 35° with a radius of curvature 25.4 mm. The second bend is 45° with a radius of curvature of 50.8 mm. The "nose" region of the middle paddles has a rectangular section 52 mm long and finishes off with a truncated triangular section 41 mm long. On the outer paddles, the "nose" section is a triangle about 30.0 mm long. The 127 mm long light guide tapers within a quasi-adiabatic cross-section of the scintillator to the 15 mm diameter Hamamatsu 10-stage R4125HA photomultiplier tube. Such long thin paddles present a formidable challenge in obtaining enough useful light. Monte Carlo calculations of the light-collection efficiency have shown that this

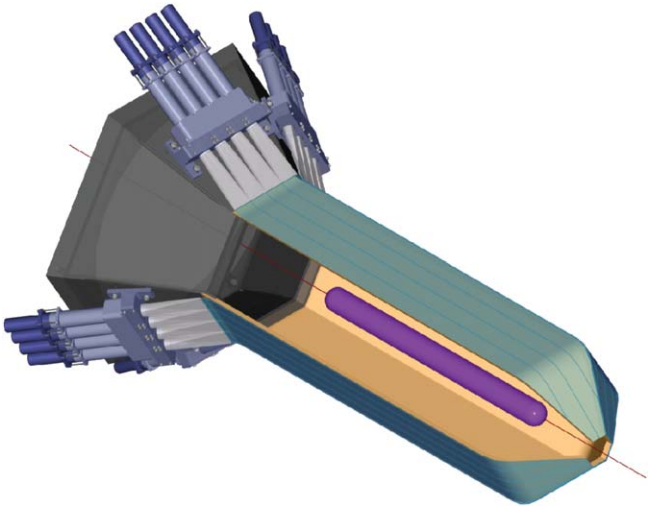

Fig. 1. New Start Counter.

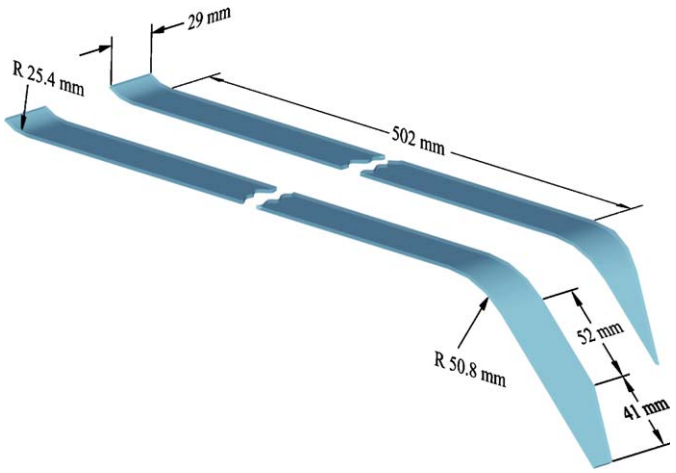

Fig. 2. New Start Counter, slat detail.

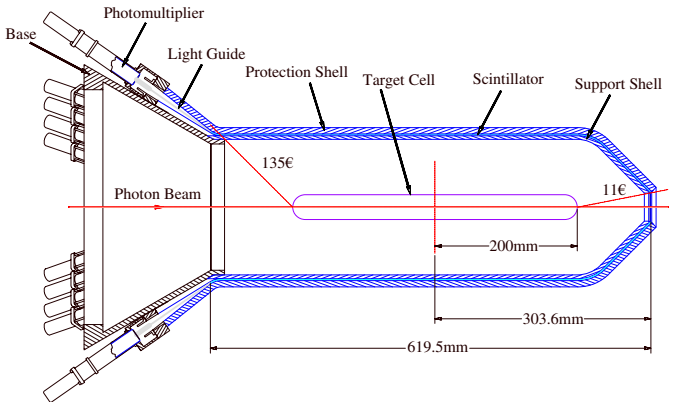

Fig. 3. New Start Counter, cross-section.

scintillator paddle's geometry would provide adequate time resolution (see Appendix A). Nevertheless, careful consideration of the wrapping to be used was needed. Tests of various wrapping materials were performed [11]. These tests are summarized in Appendix B. On the basis of these wrapping tests the paddles and light guides were wrapped in radiant mirror film VM-2000 from 3M. In addition, every other scintillator was wrapped in black Tedlar film. To avoid wrinkles and to provide smaller gaps between slats a special technology of thermal shaping of the wrapping on a mandrel has been developed and used. The hermeticity of the final assembly was estimated by direct measurements to be not less than 98%.

Each of the six sectors were assembled separately and then mounted on a rigid hexagonal support shell with 5.3-mm-thick walls made of high-strength Rohacell PMI foam with 110 mg/cm^2 density. The sag measured at the downstream end of the fully assembled Start Counter was less than 0.1 mm. The base with flange, light guides, photomultiplier tubes and various housing parts were completely out of the useful acceptance of CLAS, see Fig. 3. A schematic cross-section of the components including the wrapping that were within the acceptance

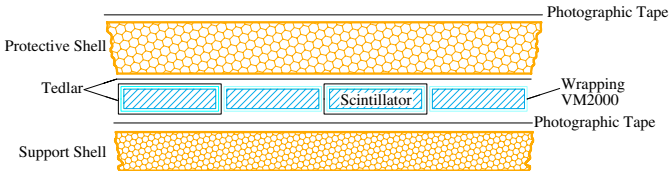

Fig. 4. New Start Counter, paddle cross-section.

are shown in Fig. 4. Their specifications are listed in Table 1. Another Rohacell PMI foam shell, 9.79 mm thick with a density of 30.0 mg/cm^3 provided further support and protection of the scintillators. The total thickness of the two shells and scintillators is 510 mg/cm^2, compared to the 660 mg/cm^2 of the scintillator and beam pipe for the previous Start Counter.

3. New Start Counter tests and performance

3.1. Preinstallation tests

Due to time constraints, only general tests were performed on the new device before installation in the experimental Hall. The relative gains were roughly measured using a ^{90}Sr electron source (2.283 MeV endpoint energy). The source was placed near the center of each paddle in coincidence with a small scintillator paddle on the other side. The energy of the electron in the paddle was 1–2 MeV, close to the minimum ionizing value, giving an energy loss of 0.43 MeV for normal incidence. The gains were equalized by adjusting the high voltage. Then the pulse height versus position was measured for one paddle (#3 of sector 21). This paddle had a PMT that had been gain calibrated according to the procedure described in Appendix B. The scale factor to convert ADC channels to photoelectrons was measured to be 0.170 ± 0.002. The pulse height versus position, measured from the light guide is shown in Fig. 5. The measured number of photoelectrons at $Z = 12$ cm was 129 p.e.

The measured attenuation length (Technical Attenuation Length, TAL) is defined as the length required to reduce the signal amplitude by $1/e$. This length is due to three factors, (a) the bulk attenuation length, (b) the thickness and shape of the scintillator and (c) the reflective properties of the surfaces. The TAL (106 cm) was surprisingly short given that the bulk attention length has a nominal value of 350 cm. To attempt to understand the value of the TAL the scintillator response was studied using a Monte Carlo program BARTIM (see Appendix A). A Landau distribution was used to generate the energy loss spread of the electrons. The energy loss was corrected for path length by averaging over the angles subtended by the coincidence paddle. The quantum efficiency of the photocathode was assumed to have a nominal value of 25%. The value for the first term in the TAL was taken to be 350 cm (see Appendix A). The second term is reproduced by the Monte Carlo program. The third term can be modelled by reducing the

Table 1
Components and wrapping materials used in Start Counter

Items	Brand name	Material	Thickness (mm)	Density (mg/cm^3)
Support shell	Rohacell XT-110	Polymethacrylimide (PMI) foam	5.33	110
Protection shell	Rohacell XT-30	Polymethacrylimide (PMI) foam	9.75	30.9
Scintillator	EJ-200	Polystyrene	2.15	1032
Radiant mirror film	VM-2000	Polyethylene Naphthalate	0.063	1300
Light insulation film	Tedlar	Polyvinyl fluoride (PVF)	0.050	1150
Light insulation tape	Photographic tape	Cotton	0.270	1020

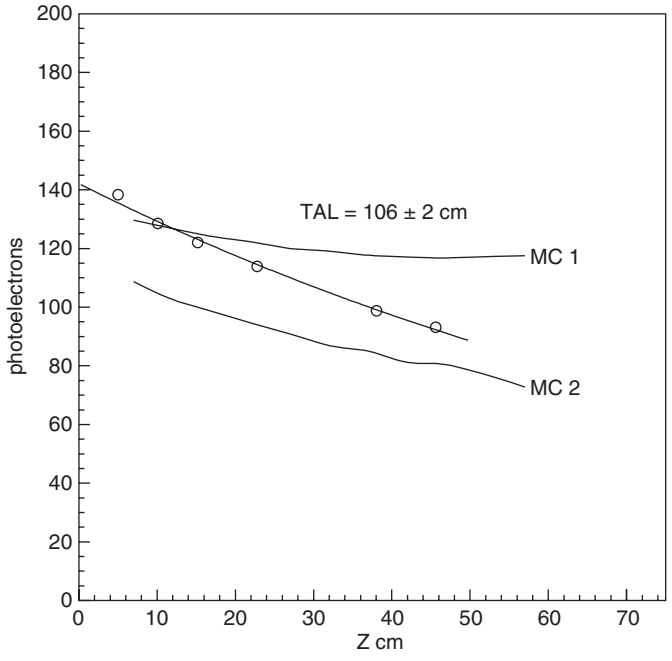

Fig. 5. Pulse height versus Z, where Z is measured from the light guide. Data taken with ^{90}Sr source. The TAL is calculated from an exponential fit to the data. The Monte Carlo simulation is shown for $R = 0.90$ and IR1 = 0.997 (MC1), and for IR1 = 0.995 in the body and IR2 = 0.950 in the bend region (MC2).

reflectivity to less than 100% for angles less than the critical angle. The pulse height at small values of Z could be reproduced by using a reflectivity for the wrapping of $R = 0.90$ and a reflectivity IR1 = 0.997 for angles less than the critical angles. These results are plotted in Fig. 5. But as can be seen in the figure, this gave a much larger TAL than the observed value. During assembly it was noted that there was marring in the region of the bends, possibly due to overheating during bending. In order to model this, the scintillator total internal reflectivity was decreased for the bend region. This is shown in the figure for IR1 = 0.995 for the body of the scintillator and IR2 = 0.950 for the bend region. This gives a better approximation for the TAL, but gives too small a pulse height.

The effect of changing the reflectivity in the bend regions is illustrated in Fig. 6. Decreasing the reflectivity in the 45° bend region, reduces the pulse height throughout the length of the scintillator since it attenuates the light reflected from the nose of the scintillator. This primarily decreases the reflected peak. For the parameters $R = 0.90$, IR1 = 0.995 and IR2 = 0.950, the Monte Carlo can approximate the slope but underestimates the pulse height by ~20%. The pulse height is affected by the photocathode efficiency, the energy loss, and the value of R used. The errors on these quantities are estimated to be about 15% for the photocathode efficiency, 8% for the energy loss and 3% for the reflectivity R, see Appendix B. This gives a total error of 17%. Another possible reason is that the light guide is approximated by a rectangular wedge, instead of an adiabatic transition from a rectangle to a circle. The Monte Carlo predicts a 40% decrease in light transmission, of which about 20% is due to the ratio of the area of a circle with radius r to the area of a square with a side of length $2r$.

All paddles, with one exception, performed adequately, although there were variations in the TAL (see Section 3.3 for more details). Given the severe time constraints, the defective paddle could not be replaced. Since it was an edge paddle, this results in only about a 3% loss of acceptance (the outer half of the edge paddles are shadowed by the magnet coils). From the data shown in Fig. 6, we can see that the paddles can deliver the ~100 p.e. needed to achieve the timing goals. Thus, the new Sart Counter was judged to be ready and it was installed in the CLAS detector.

3.2. Trigger logic

The trigger electronics must reduce the ~100 kHz hadronic interaction rate in the target to the few kHz rate that can be accepted by the data-acquisition system (DAQ). This can be achieved by selecting specific event topologies and limiting the energy range of the incoming photons that produce a trigger. The Start Counter is a fundamental tool to define the trigger for photon runs as shown in the block diagram in Fig. 7 [12]. The Start

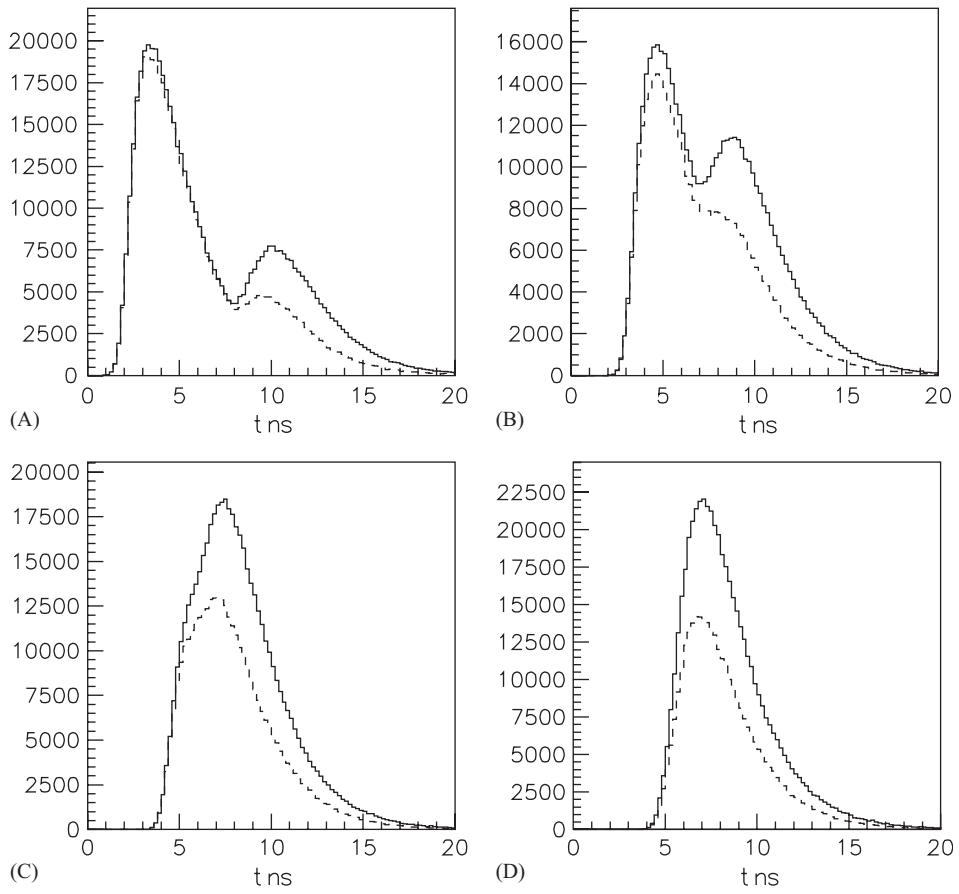

Fig. 6. Pulse height versus t. The Monte Carlo simulation of the arrival time of the photons at the cathode is shown for $R = 0.90$ and IR1 $= 0.995$ (solid line) and IR2 $= 0.950$ in the bend region (dashed line). The normally incident pion is assumed to interact at: (A) $Z = 5$ cm, (B) $Z = 25$ cm, (C) $Z = 45$ cm and (D) $Z = 55$ cm.

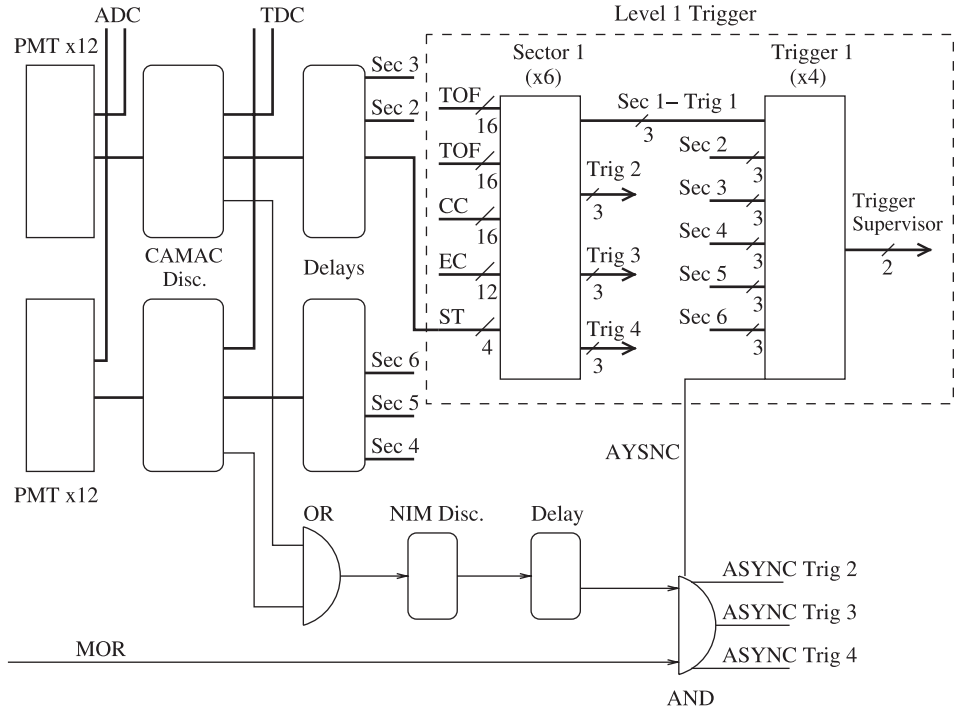

Fig. 7. Block diagram of trigger logic. For each sector the 4 Start-Counter-discriminated PMT signals, along with the corresponding TOF, EC and CC PMT signals, are fed into a synchronous memory lookup unit of Level 1 trigger. If the desired topology is found, a Trigger signal is generated. The Trigger signal from all sectors and the ASYNCH MOR-ST coincidence signal are fed into a final memory lookup unit. If the logic requirements are met a signal is passed to the trigger supervisor, which initiates the digitization and readout of the event.

Counter signals are used in two separate legs of Level 1 trigger: the synchronous leg which selects the topology of the event and the asynchronous leg that provides a fast coincidence between the OR of the tagger T-counters and the OR of the Start Counter paddles.

Level 1 trigger is deadtimeless, processing all prompt PMT signals (TOF, Calorimeter, Cherenkov detectors and Start Counter) through a pipelined memory lookup within 90 ns [1]. The PMT signals are presented to six boards corresponding to the six independent sectors and defining sector-based coincidences. The signals set bits corresponding to the active PMT's and a fast lookup table is used to determine if the required topology is met. The resulting signals, in coincidence with the asynchronous signal, are sent to the trigger supervisor, where they are used to "gate" the front-end electronics. This includes generating the common start signal for the PMT TDCs, the integrating gate signal for the PMT ADCs, and with some delay added, the common stop signal for the drift chamber TDCs. After Level 1 trigger has occurred, the event will be digitized and read out.

The dynode and anode signals from the 24 Start Counter PMTs were sent to ADCs and CAMAC C207 discriminators. The discriminated outputs were sent to both the VME V775 TDC modules and to the trigger logic. These 24 signals were combined in an OR circuit and ANDed with the MOR signal from the tagger to form the fast asynchronous (ASYNC) input of Level 1 trigger logic. The MOR (Master OR) is the OR of the tagger T-counters. The entire focal plane (64 T-counters) was on and recorded in the readout chain, but only the first 40 T-counters were enabled in the MOR. In this way we required a minimum energy in the trigger of 1.5 GeV while the low-energy photons were still available for off-line analysis. To reduce the coincidence window between the CLAS and the tagger we required the MOR signal to be in coincidence with the Start Counter OR within a time window of 15 ns.

Level 1 trigger required at least two sector-based coincidences between any of the four Start Counter paddles with any of the 48 TOF paddles, within a coincidence window of 150 ns. This width was chosen to accommodate the TOF spread of the particles hitting the TOF paddles after the ~4 m path length. We also implemented a minimum bias trigger ignoring the Start Counter and only requiring the coincidence of the TOF paddles in one or two CLAS sectors. Due to the high rates these triggers were prescaled by a factor of 10,000 and 1000, respectively. The performance of the trigger system as a function of the beam current is shown in Fig. 8. The radiator was 8×10^{-5} radiation lengths thick and the target was 40 cm of liquid

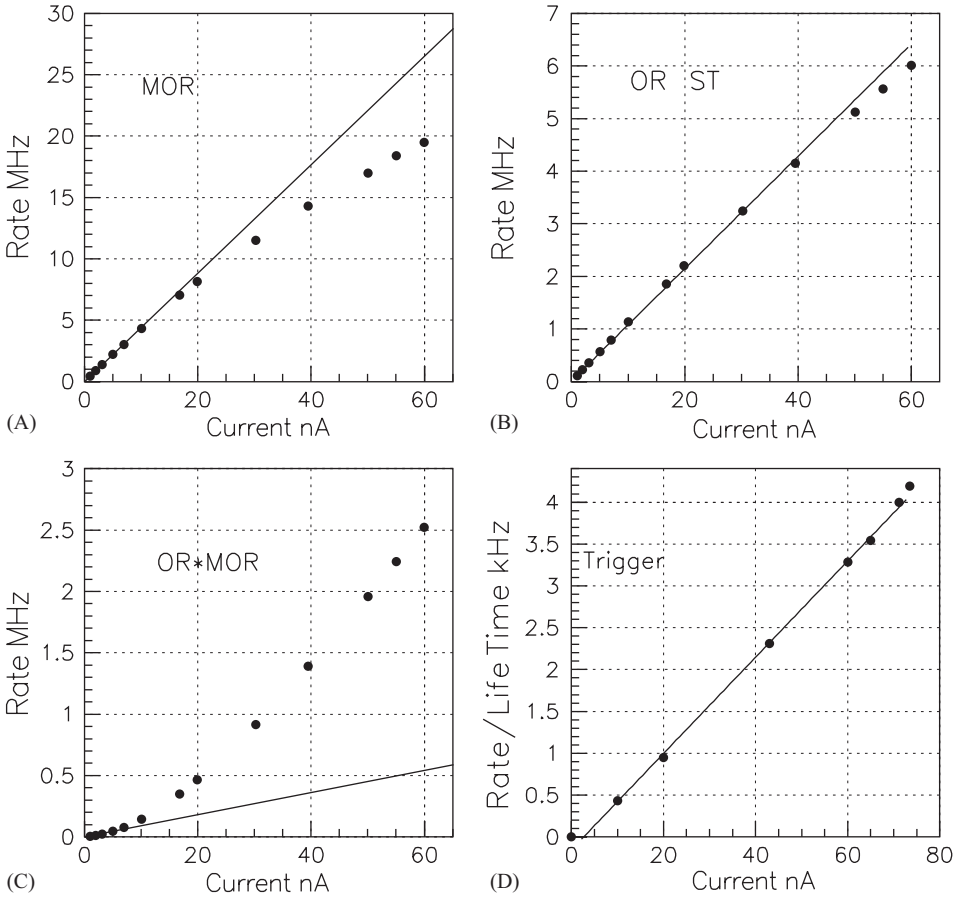

Fig. 8. PMT and trigger rates as a function of beam current. (A) MOR—the OR of the tagger T-counters, (B) OR ST—the OR of the Start Counters, (C) OR * MOR—the coincidence of the MOR and OR ST. This is the ASYNC signal and (D) Trigger—the trigger rate before the DAQ dead time.

Table 2
Summary of Level 1 trigger rates for electron and real photon running scaled to the design luminosity of $2 \times 10^{34}\text{cm}^{-2}\text{s}^{-1}$-nucleon

Trigger configuration	Electron (15.8 nA)	Real photon (162 nA)
L1(SC * EC)(SC)(SC)	39.4 kHz	
L1(SC * ST)(SC * ST)(ST) + (SC * ST)(SC * ST * ST)		11.4 kHz
L1(SC * ST)(SC * ST)(SC * ST)		1.3 kHz

hydrogen. At 60 nA the tagger signal (MOR) was beginning to saturate, providing an upper limit on the useful beam current for this configuration. However, the trigger rate remains linear up to 80 nA.

Further evidence of the efficacy of the segmented Start Counter is illustrated from the results of the trigger studies for CLAS Experiment 04-010 [13]. This experiment required a very high luminosity of $2 \times 10^{34}\text{cm}^{-2}\text{s}^{-1}$-nucleon. Two beam conditions were studied, a virtual photon beam (electrons on the target) and a real photon beam. The Start Counter is not installed during electron beam running [1]. The trigger required a track in three separate sectors, and a coincidence with the Electromagnetic Calorimeter for one sector. The EC threshold was set for a minimum ionizing particle, which selects a forward going ($<45^\circ$) fast particle. The electron was not required and was assumed to go down the beam pipe. The trigger rate, extrapolated to the desired luminosity, is given in Table 2.

For the real photon running, two trigger configurations were investigated. The first was an OR of a track in any two sectors plus an additional Start Counter hit in a third sector, and a track in one sector and two tracks in another. This was possible because the segmented Start Counter provided ϕ granularity in Level 1 trigger for the first time. The other trigger was a track in any three sectors, corresponding roughly to the electron trigger. The trigger rates are given in Table 2. Although the two beam conditions are only vaguely similar, it is clear that the addition of the Start Counter to Level 1 can reduce the trigger rate by as much as an order of magnitude.

3.3. Performance

Once the new Start Counter had been installed in CLAS, a final adjustment of the HV was made to equalize the signals in all the ADC spectra. The pulse height as a function of position was measured for all the paddles using particles from the target. However, in this case the PMT's have not been calibrated, so only relative pulse heights were measured. Positive pions with momentum in the minimum ionizing range 0.3 to 0.7 MeV/c were selected. The pulse height was measured in ± 2.5 cm bins in Z, at nine distances from the light guide. The results were corrected for the angle of incidence to give the equivalent pulse height for normally incident particles. The TALs were derived with an exponential fit to the paddle data. The results are given in Table 3. The value of TAL varies from paddle to paddle, with an average value of 163 cm, presumably due to the varying quality of the scintillator surface in the bend region. One paddle, sector 3 number 1, was apparently so badly overheated during the bending that it was unusable. Paddle number 4 in sector 6 has an unusually large TAL. Due to the complex geometry of the

Table 3
Measured TAL's for all paddles

Sector	Paddle 1	Paddle 2	Paddle 3	Paddle 4
1	121±2	156±2	155±4	87±2
2	169±5	145±3	101±2	153±3
3	36±1	176±7	137±9	192±8
4	199±8	157±5	196±10	170±7
5	141±5	157±8	226±12	194±7
6	119±4	184±6	156±7	394±34

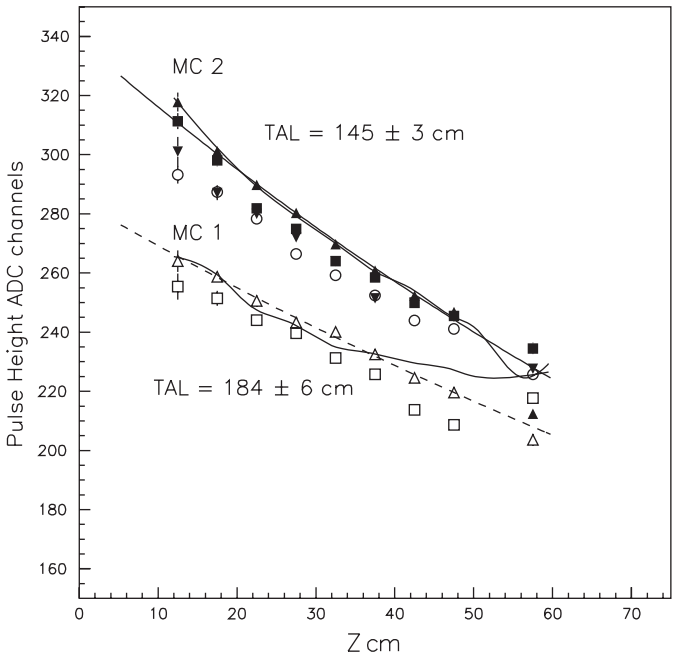

Fig. 9. Pulse height versus Z for π^+ with momentum 0.3–0.7 MeV/c. The central paddle #2 is shown for each sector. The sectors are #1 filled square, #2 filled triangle, #3 inverted filled triangle, #4 open circle, #5 open square, and #6 open triangle. A fit to the TAL is shown for sectors #2 and #6. The Monte Carlo simulation is shown for $R = 0.90$ and IR1 = 0.995 and either IR2 = 0.995 (MC1) or 0.950 (MC2) in the bend region.

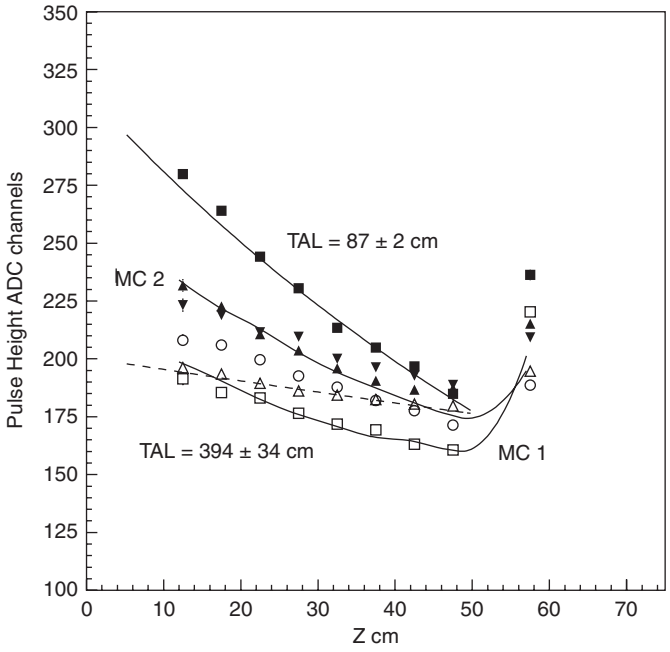

Fig. 10. Pulse height versus Z for π^+ with momentum 0.3–0.7 MeV/c. The edge paddle #4 is shown for each sector. The sectors are #1 filled square, #2 filled triangle, #3 inverted filled triangle, #4 open circle, #5 open square, and #6 open triangle. A fit to the TAL is shown for sectors #1 and #6. The Monte Carlo simulation is shown for $R = 0.90$ and IR1 = 0.995 and either IR2 = 0.995 (MC1) or 0.950 (MC2) in the bend region.

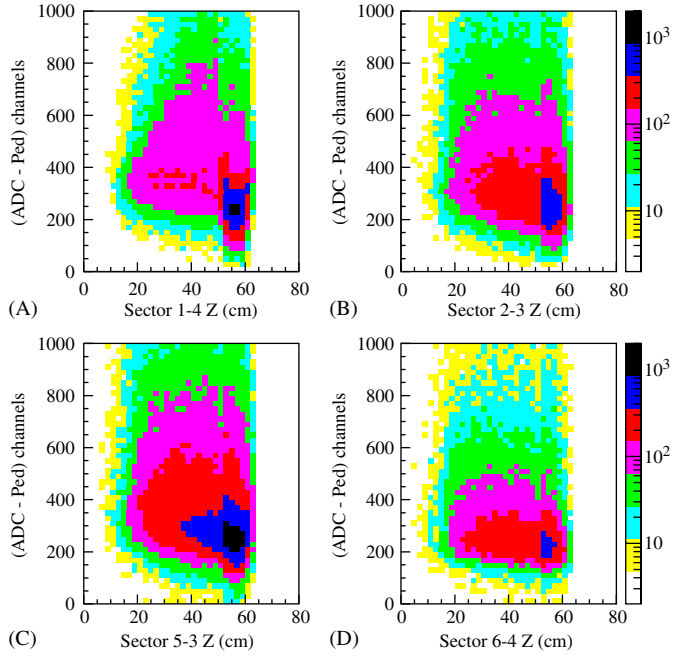

Fig. 11. The pedestal subtracted pulse height versus Z for typical paddles. (A) and (B) are edge paddles, (C) and (D) are central paddles. The distance is measured from the light guide.

paddles an exponential fit gives only an approximation of the TAL, although a useful one.

The results for one paddle from each sector are shown in Fig. 9 for central paddles and in Fig. 10 for edge paddles. All the paddles have approximately the same pulse height at large Z. This can be understood by looking at the pulse height versus Z shown in Fig. 11. The intercepted flux is much larger for $Z > 50$ cm where the paddles bend towards the beam line. Thus, when the paddle gains were equalized, we were in effect equalizing the pulse heights at large Z. Since most of the particles are produced at small angles and achieving a high overall efficiency for each paddle was required, then such equalization seems to be reasonable. As can be seen from Fig. 11 the pulse height is above the threshold for all Z, demonstrating that the efficiency of the Start Counter paddles is close to 100%. Finally, the forward region of the edge paddles has an elevated pulse height. This is due to the triangular shape of the "nose", which tends to focus the light into the direction of the PMT. The Monte Carlo simulations are plotted for $R = 0.90$, IR1 = 0.995 for all flat sections and IR2 = 0.995 (MC1) and 0.950 (MC2) in the bend regions. Since the pulse height is not calibrated the Monte Carlo simulations were scaled to fit the paddles with the nearest value of TAL. This is more pronounced in the edge paddles, because the Z chosen lies in the triangular section, while it is still in the rectangular portion of the "nose" region for the central paddles, see Fig. 2. They are a reasonable fit to the central paddle #2 in sectors #2 and #6 in Fig. 9 and the edge paddle #4 in sectors #1 and #6 in Fig. 10. Thus, the Monte Carlo parameters chosen can reproduce some of the TAL's shown and they can be tuned to fit most slopes by varying IR2 and/or IR1. For example, the Monte Carlo curve for paddle #2 in sector #6 could be improved by decreasing IR2 to reduce the pulse height in the nose region and slightly increasing IR1 to compensate in the leg region.

3.4. Timing

The time-delay calibration for each paddle is achieved by comparing the difference of the time extrapolated from the hit position on the slat to the event vertex in the target with the RF time from the accelerator. The correct RF time bucket is determined in software from the TOF system which has, on average, a time resolution of 200 ps. The time of a particle hitting a paddle is given by

$$t = c_0 + c_1 T + t_w - t_{pos} \quad (1)$$

where c_1 is typically 0.042 ns/channel and is used to convert the raw TDC channels (T) to nanoseconds. The time-delay calibration constant, c_0, is obtained for each paddle by comparing the Start Counter time with the RF time. The time walk correction, t_w, corrects for pulse height slewing. This software correction takes the empirically determined form

$$t_w = t_{w0} + \frac{t_{w1}}{A - A_0} \quad (2)$$

where A is the pulse height (ADC counts) and A_0 is the minimum pulse height. The term t_{pos} corresponds to the

time for the light to travel from the hit position to the light guide. In the straight part of the paddle ("leg" region), t_{pos} assumes the normal linear form

$$t_{pos} = \frac{l}{V_{eff}} \tag{3}$$

where l is the distance between the hit position and the light guide. The position of the hit was extrapolated from the tracking information provided by the CLAS drift chambers. V_{eff} denotes the effective velocity of the light propagation in the scintillator in the "leg" region. Fig. 12 shows the time versus position in a typical paddle. The time has been corrected for pulse height slewing and for the transit time of the particle from the interaction point in the target to the paddle. The slope gives the velocity of propagation of the light. The transit time is the time measured by the paddle minus the time of the interaction as determined by the TOF counters. In the "leg" region V_{eff} is typically 13 ± 1 cm/ns. However, the light travels in a more complicated manner when the particle hits the "nose" region. The Monte Carlo BARTIM indicates that due to the fact that the light can reflect off the triangular portion of the scintillator, resulting in a longer effective path length, one can no longer assume a linear relationship between the travel time and the distance. The following empirical form was used:

$$t_{pos} = \frac{l_0}{V_{eff}} + k_0 + k_1 l_2 + k_2 l_2^2 \tag{4}$$

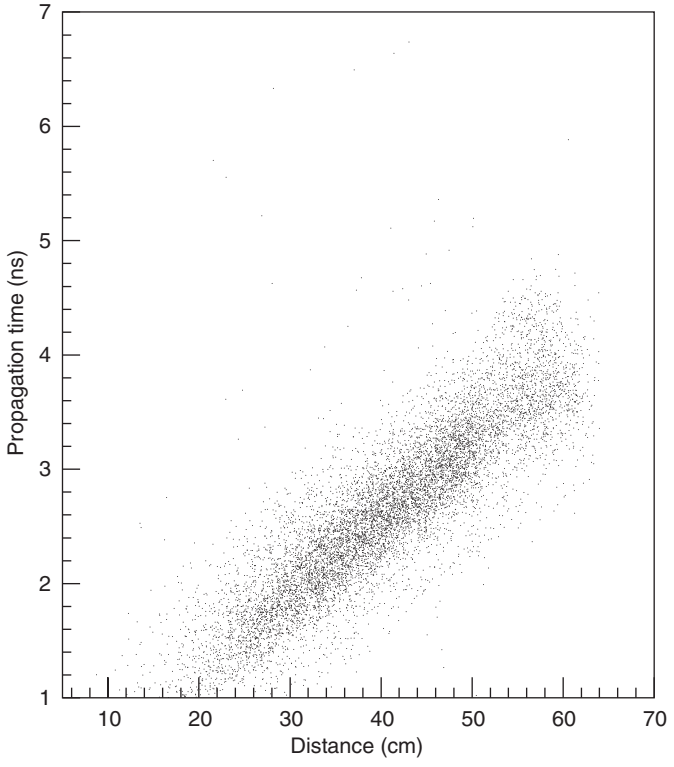

Fig. 12. Determination of the velocity of propagation of light in a Start Counter paddle. The Z-position is measured with respect to the phototube as determined by the tracks reconstructed by the CLAS tracking system.

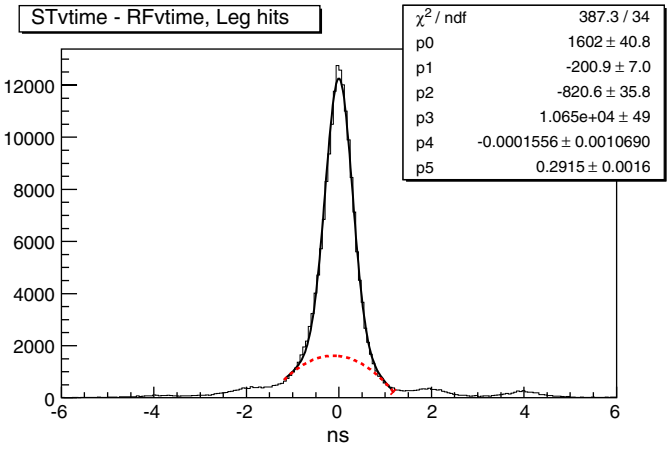

Fig. 13. Time resolution of the Start Counter for hits in the "leg" region of a paddle measured with respect to the RF time.

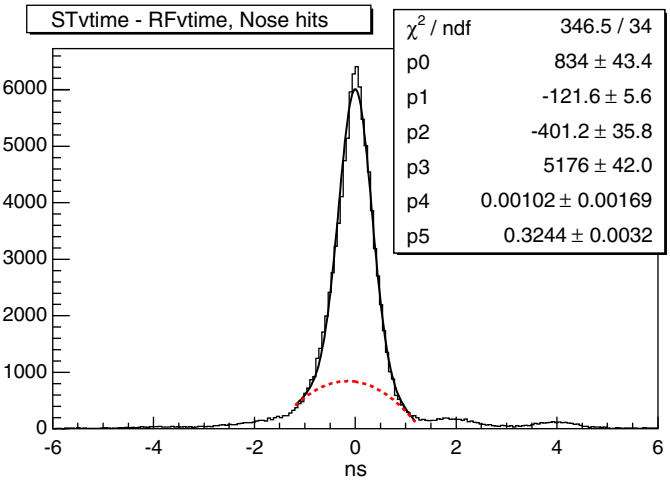

Fig. 14. Time resolution of the Start Counter for hits in the "nose" region of a paddle measured with respect to the RF time.

where the first term is due to the light propagation the whole leg length ($l_0 = 52.9$ cm), and the last three terms are due to the light propagation in the "nose" region using a second-order polynomial function of the distance, l_2, from the hit position to the leg/nose junction.

The measured time resolution of the Start Counter can be determined by fitting the time difference between the Start Counter vertex time and the RF vertex time, as shown in Figs. 13 and 14. The solid curve is a sum of a Gaussian fit plus a second-order polynomial fit to the peak. The dashed curve is the polynomial. The time resolution of the "leg" (the flat region see Fig. 2) of a Start Counter paddle, Fig. 13, is 292 ± 1 ps, while the time resolution of the "nose" (the semi-triangular region after the bend see Fig. 2) of a Start Counter paddle, Fig. 14, is 324 ± 2 ps. The peaks have non-Gaussian tails, the dashed curves, which increase the area outside the required ± 1 ns to about 3%. However, the Start Counter is intended for use in experiments with large (>2) multiplicities.

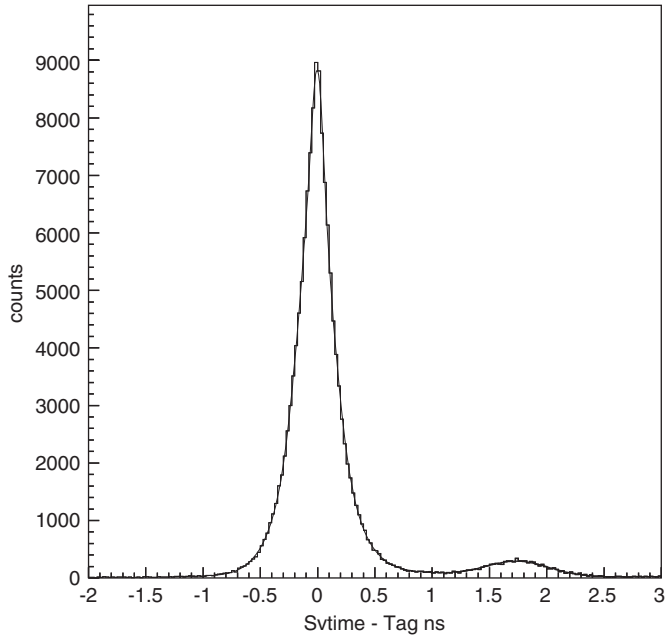

Fig. 15. Time resolution of the Start Counter for a three track vertex measured with respect to the tagger time.

Fig. 15 shows the time resolution for the vertex time of a three prong event. The side peak is due to a π^+ accidental band. Less than 0.5% of the central peak lies outside of ± 1 ns. Thus, the Start Counter essentially achieved the timing resolution goals.

4. Conclusions

A highly segmented Start Counter was designed and constructed for high-intensity photon runs at CLAS. The device was first studied based on detailed Monte Carlo simulations. These studies demonstrated that the use of long narrow single-ended paddles will give an adequate light output, ~100 p.e. This allowed the construction of a new Start Counter with a substantial increase in segmentation (24 versus 3 for the old Start Counter), without the use of an excessive number of tubes. Second, the wrapping studies clearly indicated that the new reflective material, VM2000, is superior to the standard aluminized Mylar, despite its short wavelength cutoff. Finally, the tests of the finished Start Counter showed that technical attenuation length varied by almost a factor of 2 from one paddle to another. This was attributed to non-uniformities in the scintillator bends. However, despite this problem, all paddles, except one, produced enough light to give good efficiency and adequate timing. The new Start Counter has performed well and met the timing goals, <388 ps, and efficiency goals set for it. The trigger studies clearly demonstrate the flexibility of the segmented Start Counter and its ability to reduce the trigger rate by requiring complex topologies.

Acknowledgements

We gratefully acknowledge the TJNAF Machine Shop personnel Dave McCay, Casy Apeldoorn, Gary Slack, Robert Martin and Jeffery Dail for their many contributions to the construction and design of the system. The authors would also like to thank Elton Smith, TJNAF, for many helpful discussions on the trigger system and Adam Meier and W.J. Llope, Rice University for their help with the figures. This work was supported in part by the Istituto Nazionale di Fisica Nucleare, an Emmy Noether Grant from the Deutsche Forschungsgemeinschaft, the Korean Research Foundation, the US Department of Energy and the National Science Foundation. The Southeastern Universities Research Association operates the Thomas Jefferson National Accelerator Facility for the United States Department of Energy under contract DE-AC05-84ER40150.

Appendix A. Monte Carlo BARTIM

A Monte Carlo program, BARTIM, was written to transport the light through a scintillator and attached light-guide system. The scintillator is built up of constant thickness subunits with simple geometric areas, such as rectangles, triangles, and rectangular sections bent in one dimension. Light guides are approximated by rectangular cones. The effect of wrapping the scintillator is modelled by specularly reflecting the light that escapes the scintillator with an appropriate reflection coefficient R. This makes the somewhat unrealistic assumption that the wrapping is perfectly smooth and conforms exactly to the surface of the scintillator or light guide. This program was then used to evaluate the various wrapping materials used on the simple parallelepiped test bar and the new segmented Start Counter.

The light is generated isotropically along the line of an incident charged particle (for convenience the track is split into 10 discrete points). The energy loss of the charged particle can be calculated from a Vavilov distribution, using CERN programs DINVAV and RANLAN, or assuming a minimum ionizing particle. The number of photons is calculated using 10,000 photons per MeV for BC400 (65% of Anthracene). The time spread is given by the convolution of a 0.2 ns clipped Gaussian with the rise and decay times of the scintillator [14]. The 0.2 ns represents the decay time of the excited benzene ring and the other two times are the decay times of the phosphors used to downshift the UV photon to blue light which can be seen by the PMT. The time of each photon is then tracked through the system according to the path length and index of refraction, which is 1.58 for the scintillators in Table A.1. The attenuation of the photon is modelled by

$$P(L) = \exp(-L/D) \tag{A.1}$$

where D is the absorption length of the material being transversed. The properties of various scintillators are given in Table A.1.

Table A.1
Scintillator properties

Scint	Wave length of emission (nm)	Light output anthracene (%)	Rise time (ns)	Fall time (ns)	Bulk atten. length (cm)
BC408	428	64	0.9	2.1	380
BC404	408	68	0.7	1.8	160
BC420	391	64	0.5	1.5	110
EJ200	428	64	0.9	2.1	300–400

A photon is then tracked until it hits a wall. It is either totally internally reflected, or reflected or refracted according to the Fresnel equations

$$R(\alpha) = \tfrac{1}{2}[\sin^2(\alpha-\beta)/\sin^2(\alpha+\beta) + \tan^2(\alpha-\beta)/\tan^2(\alpha+\beta)] \quad (A.2)$$

where we have assumed an equal mixture of polarizations. The incident angle, normal to the interface, is given by α and the refracted angle is given by β. Imperfections on the surface can be modelled by reducing the total internal reflection coefficient, IR, below 100%. The light that escapes the scintillator is specularly reflected with an appropriate reflection coefficient R. Photons that are absorbed or lost are removed and tabulated. If the wall is an interface between the scintillator and light guide, Snell's law is used to give the angle of the refracted photon. The time of each photon is then tracked through the system according to the path length and index of refraction, which is 1.58 for the scintillators in Table A.1. The process is repeated for several hundred photons to gain decent statistics, but the results are reported per event. Finally, the number of photons must be converted to photoelectrons from the photocathode. For the R4125 PMT being tested here, a nominal conversion factor of 0.25 is used.

Appendix B. Wrapping tests

Since the long thin paddles present such a formidable challenge in obtaining enough useful light, careful consideration of the wrapping to be used was needed. Tests of various wrapping materials to be used in conjunction with the EJ2000 scintillator were performed. Further details are given in Ref. [11]. The materials tested were two samples of a highly reflective non-metallic multilayer polymer developed by 3M. This material has >95% reflectivity in the visible but decreases to less than 50% below 400 nm. Since the emission spectrum of EJ2000 extends below 400 nm, measurements of the effective reflectivity were needed. Two samples VM2000, 2.5 mil thick, and VM2002, 1.5 mil thick were evaluated. The two samples were compared with a standard material, aluminum coated Mylar, 1 mil thick. The tests were performed using cosmic rays, to simulate minimum ionizing particles.

The setup consisted of two scintillators overlapped to form a 1.25 in. × 1.25 in. active area to tag a cosmic ray event. This yielded a rate of about 2 counts/min. The test scintillator, with dimensions 12 in. × 1 in. × 2 mm, was placed between the two paddles at its midpoint and read out without forming a three-fold coincidence. The test scintillator was coupled to a Hamamatsu R4125 10-stage PMT. It has a 15 mm active area diameter so that less than 60% of the light generated in the 25.4 mm wide scintillator is collected. The scintillator could not be glued to the PMT since it had to be available for later use. Thus, it was difficult to provide a reliable optical coupling to the long thin scintillator without interfering with the light collection. The solution was to use a 1 mm air gap. This resulted in a factor of 2–3 less light, but was reasonably reliable. Since the number of photoelectrons with this arrangement was expected to be 100 or less, a 4x amplifier was used to boost the signal into the midrange of the ADC.

The ADC scale was calibrated using the well known statistical method [15]. The number of photoelectrons can be estimated from the signal distribution width via the formula

$$N_{\text{phe}} = G\left(\frac{Q}{\sigma_Q}\right)^2 \quad (B.1)$$

where Q is the ADC peak, σ_Q is the RMS of the peak and G is related to the gain, κ, of an individual dynode. Assuming that all 10 dynodes have the same gain, as is the case for most tubes,

$$G = \frac{\kappa}{\kappa - 1} \quad (B.2)$$

κ can be estimated from the amplification of the PMT, $\kappa \simeq K^{1/10}$. A better estimate of G can be obtained from the measurements by using the equation

$$K = \frac{\sigma_Q^2}{4eGQ} \quad (B.3)$$

and iterating. The factor of 4 is due to the use of the 4x amplifier.

The method requires a stable light source to inject a fixed number of photons into the PMT. This was provided by using a Nichia NSPB320BS blue LED. It is capable of producing a stable light output at 460 nm for short pulses, which is well matched to the PMT photocathode response. The LED was driven with a square pulse 4.5 V in amplitude with a width of 25 ns. This gave about 460 K p.e. and a long-term stability of a few percent [16]. The LED

illuminated a bundle of silica light fibers with one fiber illuminating a pinhole placed over the PMT. This gave the 100–200 p.e. that we required. A second run was made with a larger pinhole to approximately double the pulse height. The pedestal was measured to be 17 channels and the RMS spread of the pulser and 4x amplifier was measured to be 0.6%. From the data, K was estimated to be 1.74×10^6 and $G = 1.31$. Using this value, the two runs were found to have 133 and 315 p.e., respectively, which corresponds to scale factors, converting ADC channels to photoelectrons, of 0.227 and 0.224. The calibration procedure was repeated at the end of the testing, yielding 358 p.e. and a scale factor of 0.227. An average scale factor of 0.226 ± 0.002 was used to analyze the data.

Each wrapping material was tested several times to check for reproducibility of the results. In addition, runs were made with no wrapping (black paper) for a comparison with the Monte Carlo predictions and to provide a baseline to evaluate the wrapping. The pulse height spectrum of the test paddle was fit with an approximation to the Landau function

$$f(\mathrm{ADC}) = A\exp[(B-\mathrm{ADC})/2C - \exp\{(B-\mathrm{ADC})/C\}] + D \quad \text{(B.4)}$$

where ADC is the ADC channel and A, B, C, and D are varied. The peak is given by $B + C\ln(2)$. This gives the most probable value. The typical ADC spectra and fits are shown in Fig. B.1.

The results from several runs are listed in Table B.1, in which the scintillator was rewrapped in each case. As the light leaves the end of the scintillator, it is refracted to larger angles and spreads out in space. Thus, the light hitting the PMT will decrease with increasing spacing. But tests show that as long as the scintillator to PMT distance is less than 2 mm the results are reproducible to 3%, which corresponds to a systematic error of about ~2 p.e. As can be seen from these data, both VM2000 and VM2002 give superior results compared with aluminized Mylar and are roughly equal within the errors of the measurement.

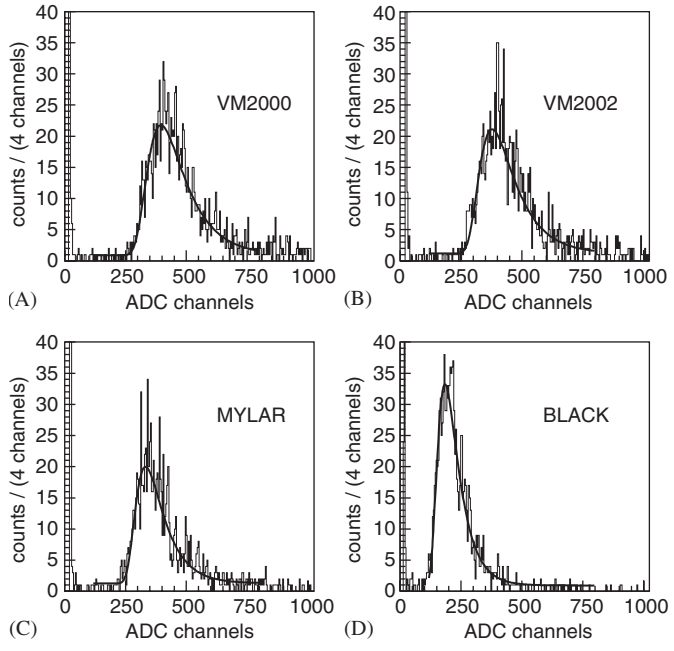

Fig. B.1. Test paddle pulse height spectrum. The scintillator is wrapped with (A) VM2000, (B) VM2002, (C) Mylar and (D) Black Paper.

Table B.1
Measured pulse heights, in units of photoelectrons, for the various wrapping materials. Values given are for the most probable energy loss

	VM2000	VM2002	Mylar	"Black"
1	73.1±0.7	74.6±0.8	67.7±0.8	40.8±0.5
2	72.2±0.7	74.6±0.7	69.8±0.5	47.1±0.6
3		75.0±0.6		
Avg.	72.7±0.5	74.7±0.3	69.2±0.4	43.8±0.4

In order to estimate the reflectivity of a given wrapping we must compare the measured pulse height to a Monte Carlo simulation as a function of the reflectivity. But the Monte Carlo requires several input parameters that are not well known. Specifically, we need to know the photocathode efficiency, the attenuation length, internal reflectivity factor IR and the energy deposited in the scintillator. From the phototube data sheets, the quantum efficiency of the photocathode was assumed to have a nominal value of 0.25 and the bulk attenuation length was assumed to be 350 cm, midway between 300 and 400 cm. Additional information was obtained by measuring the attenuation length of the bar using a ^{109}Ru beta source, with an endpoint energy of 3.54 MeV. A Landau distribution was used to generate the energy loss spread of the electrons. This value was corrected for path length by averaging over the angles subtended by the coincidence paddles. Since we do not have a monochromatic normally incident beam the average amount of energy deposited in the scintillator represents the largest potential error in this calculation. We estimate about a 3–4% error due to the energy spread and about 8% due to the angular spread of the electron beam. The photocathode quantum efficiency varies from about 0.3 at 400 nm to 0.2 at 480 nm, the region of the scintillator emission spectrum. An effective value of 0.25 was used in the Monte Carlo calculations. According to the manufacturer the variation in the cathode blue sensitivity at 400 nm is about 15%. Since the peak of the scintillator spectrum is near 400 nm this should give a reasonable estimate of the quantum efficiency variation. The source was placed directly on the test scintillator, 1.5, 6.0 and 10.5 in. from the PMT and a coincidence with the lower paddle was formed. The pulse height versus position is shown in Fig. B.2. An exponential fit to the data gives a TAL of 230 cm for the Mylar wrapping and 275 cm for the VM2000 wrapping. These results could be reproduced by assuming that the reflectivity (R) was 0.70 for Mylar and 0.90 for VM2000. In both cases the internal reflectivity (IR) was

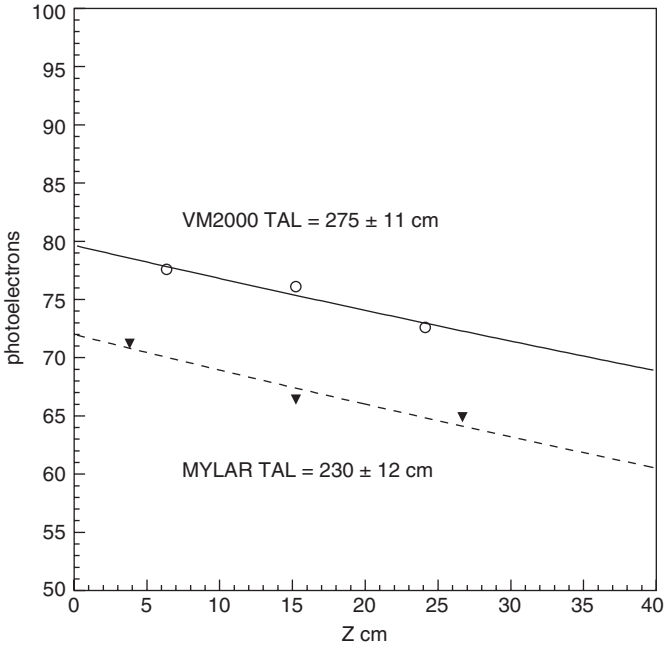

Fig. B.2. Number of photoelectrons versus distance from the PMT. The top curve is for a VM2000 wrapping and the bottom curve is for aluminized Mylar wrapping. The data were taken with a ^{109}Ru source. The effective attenuation length (TAL) is given for the two cases.

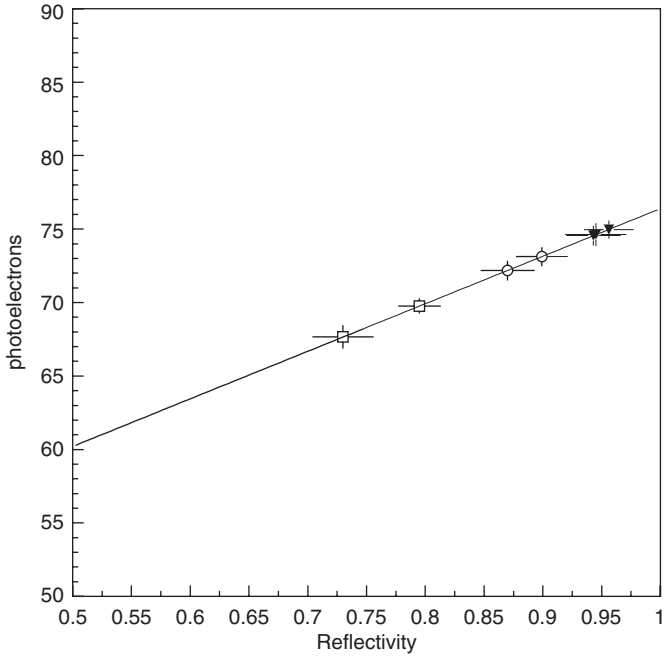

Fig. B.3. Measured photoelectrons versus reflectivity. The curve is the Monte Carlo values for minimum ionizing cosmic rays. Open circles are VM2000, filled triangles are VM2002 and open squares are aluminized Mylar.

taken to be 99.5% instead of 100%. This accounts for any imperfections of the scintillator surfaces. With these assumptions the data and Monte Carlo can be brought into agreement. However, the system is not well determined. For example, if the bulk attenuation length is 300 cm instead of the 350 assumed, the value of IR would be approximately 99.6%.

The Monte Carlo calculation of the number of photoelectrons versus reflectivity of the wrapping material is plotted in Fig. B.3. The value for the attenuation length and internal reflectivity found above were used. The Monte Carlo was normalized by setting the number of photoelectrons at zero reflectivity to the value measured for the "Black" wrapping, e.g. 44 p.e. The data tabulated in Table B.1 are plotted at the value of the reflectivity corresponding to the number of photoelectrons measured. The average values of reflectivity, R, for the VM2000 is 0.89 ± 0.02, VM2002 is 0.95 ± 0.01 and Mylar is 0.78 ± 0.02. The reflectivity of the VM2000 and VM2002 should be identical since they differ only in the thickness. The two Mylar runs also differ by more than the statistical errors. These discrepancies are presumably due to the 3% systematic error in the optical coupling due to the spacing variation.

References

[1] B. Mecking, et al., Nucl. Instr. and Meth. A 503 (2003) 513.
[2] M.D. Mestayer, et al., Nucl. Instr. and Meth. A 449 (2000) 81.
[3] E.S. Smith, et al., Nucl. Instr. and Meth. A 432 (1999) 265.
[4] G. Adams, et al., Nucl. Instr. and Meth. A 465 (2001) 414.
[5] M. Amarian, et al., Nucl. Instr. and Meth. A 460 (2001) 239.
[6] D.I. Sober, et al., Nucl. Instr. and Meth. A 440/2 (2000) 263.
[7] S. Taylor, et al., Nucl. Instr. and Meth. A 462 (2001) 484.
[8] T. Smith, J. Distelbrink, G. Briggs, A 'Coupled-Paddle' Design for the Start Counter of CLAS. CLAS-Note 95-003.
[9] V. Kubarovsky, et al., Phys. Rev. Lett. 70 (2004) 014005; S. Stepanyan, et al., Phys Rev. Lett. 91 (2003) 252001.
[10] M. Ripani, M. Battaglieri, R. De Vita, Simulation of Photon Beam Interactions on a Hydrogen Target for Future Experiments. CLAS-Note 2005-006.
[11] G.S. Mutchler, Y. Sharabian, Wrapping Tests and Monte Carlo evaluation of a new Highly Segmented CLAS Start Counter. CLAS-Note 2005-008.
[12] M. Battaglieri, R. De Vita, V. Kubarovsky, Spectroscopy of Exotic Baryons with CLAS: Search for Ground and Excited States, CLAS Experiment 04-021.
[13] E. Smith, S. Stepanyan, V.N. Batourine, Evaluation of rates during eg3 beam tests. CLAS-Note 2004-031.
[14] E. Gatti, V. Svelto, Nucl. Instr. and Meth. 43 (1996) 248.
[15] V.L. Rykov, Method for the Absolute PMT Calibration. STAR Note SN0301, August 1997.
[16] T. Nomura, T. Shinkawa, Blue LED for RS Monitor. Experiment 949 Technical Note #6, February 2000.